Received: 22 May 2023 | Revised: 22 December 2023 | Accepted: 16 January 2024

DOI: 10.1111/nan.12962

ORIGINAL ARTICLE

Neuropathology and Applied Neurobiology
JOURNAL OF THE BRITISH NEUROPATHOLOGICAL SOCIETY

WILEY

# Inflammatory bowel disease induces pathological α-synuclein aggregation in the human gut and brain

Ana M. Espinosa-Oliva[1,2] | Rocío Ruiz[1,2] | Manuel Sarmiento Soto[1,2,3] | Antonio Boza-Serrano[1,2,4] | Ana I. Rodriguez-Perez[5,6] | María A. Roca-Ceballos[1,2] | Juan García-Revilla[1,2] | Marti Santiago[1,2] | Sébastien Serres[3,7] | Vasiliki Economopoulus[3] | Ana E. Carvajal[8] | María D. Vázquez-Carretero[8] | Pablo García-Miranda[8] | Oxana Klementieva[9] | María J. Oliva-Martín[1,2] | Tomas Deierborg[4] | Eloy Rivas[10] | Nicola R. Sibson[3] | José L. Labandeira-García[5,6] | Alberto Machado[1,2] | María J. Peral[8] | Antonio J. Herrera[1,2] | José L. Venero[1,2] | Rocío M. de Pablos[1,2]

[1]Instituto de Biomedicina de Sevilla, IBiS/Hospital Universitario Virgen del Rocío/CSIC/Universidad de Sevilla, Sevilla, Spain

[2]Departamento de Bioquímica y Biología Molecular, Facultad de Farmacia, Universidad de Sevilla, Sevilla, Spain

[3]Cancer Research UK and Medical Research Council Oxford Institute for Radiation Oncology, Department of Oncology, University of Oxford, Churchill Hospital, Oxford, UK

[4]Experimental Neuroinflammation Laboratory, Department of Experimental Medical Science, Lund University, Lund, Sweden

[5]Research Center for Molecular Medicine and Chronic Diseases (CIMUS), University of Santiago de Compostela, Health Research Institute (IDIS), Santiago de Compostela, Spain

[6]Networking Research Center on Neurodegenerative Diseases (CIBERNED), Madrid, Spain

[7]School of Life Sciences, University of Nottingham, Nottingham, UK

[8]Departamento de Fisiología, Facultad de Farmacia, Universidad de Sevilla, Seville, Spain

[9]Dementia Research Laboratory, Department of Experimental Medical Science, Lund University, Lund, Sweden

[10]Departamento de Anatomía Patológica, Hospital Universitario Virgen del Rocío, Seville, Spain

**Correspondence**
Ana M. Espinosa-Oliva, Departamento de Bioquímica y Biología Molecular, Facultad de Farmacia, Universidad de Sevilla, Seville, Spain.
Email: anaespinosa@us.es

**Funding information**
Cancer Research UK, Grant/Award Number: C5255/A15935; Junta de Andalucía, Grant/Award Number: CTS 5884; Ministerio de Ciencia, Innovación y Universidades, Grant/Award Number: RTI2018-098830-B-I00; Ministerio de Economía y Competitividad, Grant/Award Number: SAF2015-64171-R; ministerio español de salud

## Abstract

**Aims:** According to Braak's hypothesis, it is plausible that Parkinson's disease (PD) originates in the enteric nervous system (ENS) and spreads to the brain through the vagus nerve. In this work, we studied whether inflammatory bowel diseases (IBDs) in humans can progress with the emergence of pathogenic α-synuclein (α-syn) in the gastrointestinal tract and midbrain dopaminergic neurons.

**Methods:** We have analysed the gut and the ventral midbrain from subjects previously diagnosed with IBD and form a DSS-based rat model of gut inflammation in terms of α-syn pathology.

**Results:** Our data support the existence of pathogenic α-syn in both the gut and the brain, thus reinforcing the potential role of the ENS as a contributing factor in PD

José L. Venero and Rocío M. de Pablos share senior authorship.

Rocío Ruiz, Manuel Sarmiento Soto and Antonio Boza-Serrano contributed equally to this work.

Ministerio de Salud, Grant/Award Number: PI17/00828; Marie Skłodowska-Curie Individual Fellowship

aetiology. Additionally, we have analysed the effect of a DSS-based rat model of gut inflammation to demonstrate (i) the appearance of P-α-syn inclusions in both Auerbach's and Meissner's plexuses (gut), (ii) an increase in α-syn expression in the ventral mesencephalon (brain) and (iii) the degeneration of nigral dopaminergic neurons, which all are considered classical hallmarks in PD.

**Conclusion:** These results strongly support the plausibility of Braak's hypothesis and emphasise the significance of peripheral inflammation and the gut-brain axis in initiating α-syn aggregation and transport to the substantia nigra, resulting in neurodegeneration.

**KEYWORDS**
alpha-synuclein, inflammatory bowel disease, neurodegeneration, neuroinflammation, Parkinson's disease

## INTRODUCTION

Parkinson's disease (PD) is an irreversible neurodegenerative disorder characterised by a selective and gradual degeneration of the dopaminergic neurons in the substantia nigra (SN) pars compacta [1]. Lewy pathology in PD includes Lewy neurites and Lewy bodies (LB), whose main component is fibrillar α-synuclein (α-syn) [2]. Braak and colleagues hypothesised that PD pathogenesis may have an origin in the enteric nervous system (ENS), gaining access to the brain through the entire gastrointestinal (GI) tract, including the axons of the myenteric (Auerbach's) plexus and/or the submucosal (Meissner's) plexus via postganglionic neurons [3]. The prospect that pathogenic α-syn may spread from the gut to the brain to cause degeneration of the nigrostriatal dopaminergic system is certainly attractive, and recent data from experimental animals support this view. Hence, injections of different forms of α-syn into the ENS wall of rodents and non-human primates induce vagal spreading of α-syn pathology to the dorsal motor nucleus of the vagus nerve (DMNV) [4–7]. These studies highlight the potential involvement of the gut–brain axis in the spread of α-syn pathology under human disease-like conditions, including PD.

Intriguingly, recent cohort studies have shown an association between PD and inflammatory bowel diseases (IBDs) [8, 9]. IBDs are common chronic intestinal diseases usually classified as ulcerative colitis (UC) and Crohn's disease (CD). A typical feature of IBD is long-lasting systemic inflammation. Consequently, with all these precedents, we wondered whether IBD is associated with the appearance of pathogenic α-syn in the GI tract and midbrain dopaminergic neurons. To this end, experimental analyses have been performed using human and animal models. Our results reinforce the importance of the gut–brain axis as a pathway of pathological α-syn transmission.

**Key Points**

- IBD induces phosphorylation of α-synuclein in the gastrointestinal tract.
- Animal model shows that gut inflammation induces phosphorylation of α-synuclein in the midbrain.
- Gut inflammation may spread α-synuclein pathology to the midbrain.
- IBD could be a risk factor for Parkinson's disease.

## METHODS

### Animals and treatments

One hundred five male albino Wistar rats (200–300 g) were used for these studies. The control group received tap water at the different time points analysed. We have used an experimental UC model, based on the oral administration of DSS (molecular weight 36–50 kDa; MP Biomedicals) at a concentration of 5% (w/v) in drinking water. Rats received different DSS regiments (28 and 63 days) depending on the technique used (Figure S1a,b). A group of animals underwent bilateral sub-diaphragmatic vagotomy (see the Supporting Information and Figure S1c).

### Human tissue samples

Human samples of inflamed colon were obtained from subjects with UC ($N = 6$). Healthy colon was obtained from subjects (control) who had undergone colonic resection to remove a tumour ($N = 6$) (Table S1). Brain human tissue was obtained from subjects who suffered ($N = 8$) or not ($N = 8$; control subjects) IBD and died from different causes (see Table S2). More information is available in the Supporting Information.

Human studies were approved by the corresponding ethic committees (authorisation code: 2051-N-20). Informed consent was obtained from all subjects.

### Immunohistological evaluation

To study the status of microglial cells and dopaminergic neurons immunological staining was performed after the different treatments

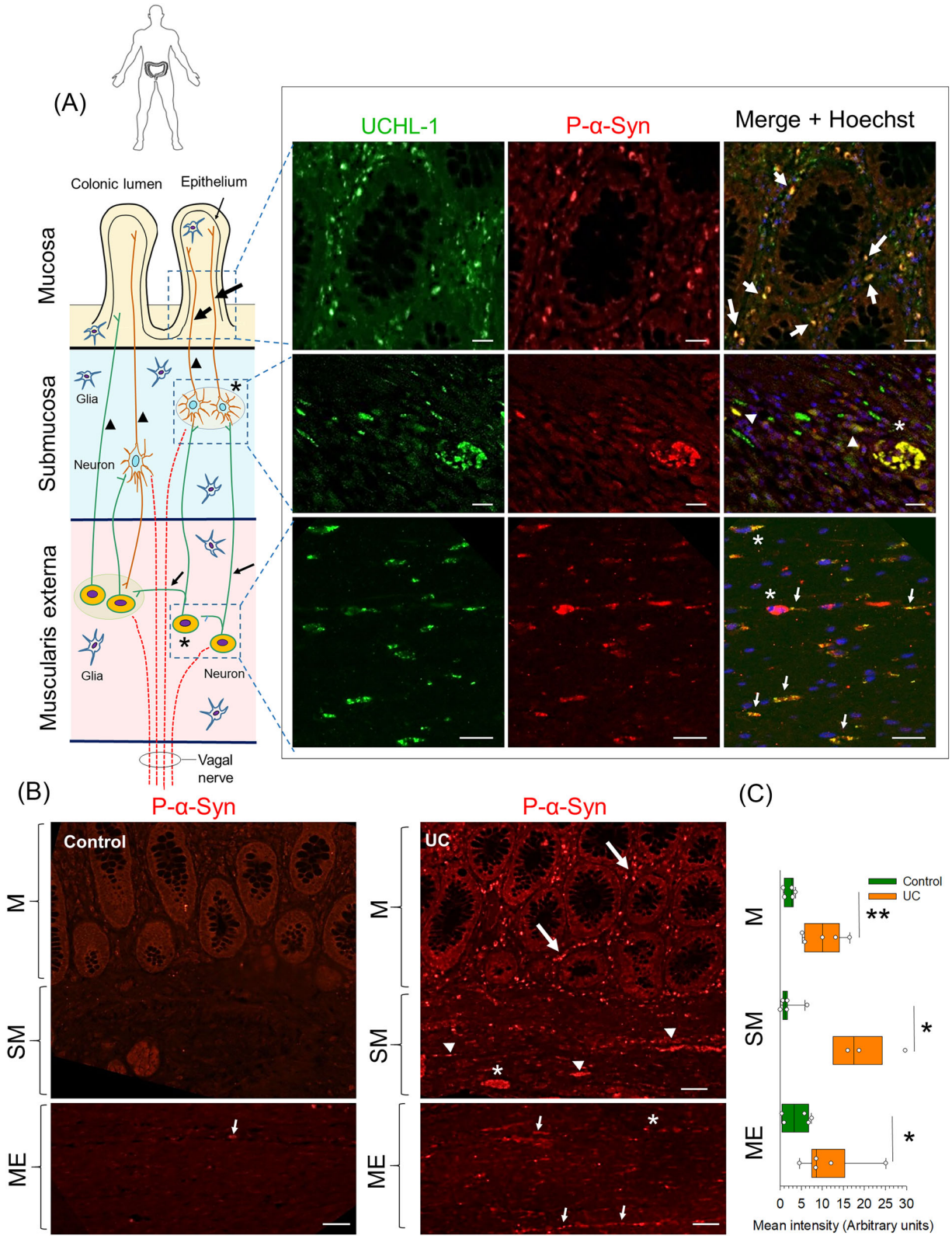


**FIGURE 1** Legend on next page.

(Figure S1). Incubations and washes were performed in Tris-buffered saline (TBS) or phosphate-buffered saline (PBS), pH 7.4, and all work was performed at room temperature (RT). The primary and secondary antibodies used are listed in Table S3. Additional details of this technique are available within the Supporting Information.

## Immunohistochemistry data analysis

Cells showing Iba-1 immunoreactivity were counted across five sections per animal, systematically distributed through the SN anterior–posterior axis (see Supporting Information). The number of tyrosine hydroxylase (TH)- and Nissl-positive neurons in the SN was estimated as detailed in the Supporting Information. For immunofluorescence quantification, images were acquired using an inverted ZEISS LSM 7 DUO confocal laser scanning microscope with the same laser intensity and gain conditions. Images were quantified using Image-J software (see the Supporting Information).

## Dot blot

To corroborate the results obtained by immunohistochemistry dot blot analysis was performed using 1 μg of tissue homogenate that was spotted in 1-μL volume aliquots onto 0.45-μm nitrocellulose membrane. Membranes were blocked with blocking solution for 2 h at RT and then incubated with primary antibodies (Table S3) in blocking solution at 4°C overnight. After washing, membranes were incubated with horseradish peroxidase (HRP)-conjugated secondary antibodies in a blocking solution for 2 h at RT. The Amersham™ Imager 600 was used to detect HRP-conjugated secondary antibodies using a chemiluminescent substrate (Biorad). Densitometry analysis was performed using ImageJ software (see the Supporting Information).

## ELISA

ELISA was performed to study the status of peripheral inflammation after DSS treatment. Fresh peripheral blood was collected from animals of the different treatment groups. Serum tumour necrosis factor (TNF) and interleukin (IL)-1β concentrations were determined by using a rat TNF alpha Uncoated ELISA and a rat IL-1β ELISA Kit (all from Invitrogen) following the manufacturer's instructions. The plates were read on a Synergy HT multimodal plate reader (BioTek, Winooski, VT, USA) set to 450 nm (see the Supporting Information).

## Magnetic resonance imaging (MRI) and regional cerebral blood volume (rCBV) map calculation and analysis

MRI allowed us to measure the effect of peripheral inflammation due to DSS treatment on the permeability of the BBB. All MRI was performed using a horizontal bore 9.4 T magnet with a Varian DirectDrive™ (Agilent Technologies). Multi-parametric MRI was performed, including the acquisition of $T_1$-weighted images pre- and post-gadolinium-DTPA injection to assess blood–brain barrier (BBB) integrity, and $T_2$-weighted images to determine macroscopic changes in tissue structure, as indicated in the Supporting Information.

rCBV maps were generated from time-series images acquired during bolus injection of contrast agent and tracer kinetic analysis. The rCBV maps were thresholded at a level that was equal to the mean signal intensity plus two standard deviations of the signal intensity of the prefrontal cortex (non-DSS-affected structure) as a reference. An in-house ImageJ plugin was used to generate the maps (see the Supporting Information). For each animal, we performed post–pre gadolinium-DTPA subtractions to generate a final map for each time point and then compare absolute intensity throughout the time course of the study.

## Quantification of peripheral immune cell infiltration by flow cytometry

Flow cytometry of SN was performed following a standard procedure using Becton Dickinson Bioscience antibodies as shown in Table S4. Cells were acquired in a FACSCanto II employing the FACSDiva software (Becton Dickinson Bioscience). Analysis was further conducted using the FlowJo software program (FlowJo LLC). Additional details of this technique are available within the Supporting Information.

## Real-time quantitative reverse transcription PCR (RT-qPCR)

The level of inflammatory mediators was measured by RT-PCR. β-actin served as the reference gene and was used for sample normalisation.

**FIGURE 1** Immunolocalisation of P-α-syn in the colon of human subjects with UC. (A) Schematic cross-section of the colon wall illustrating the interconnected enteric plexuses, which contain neurons projecting to the mucosa, and vagal fibres. Colocalisation of P-α-syn and UCHL-1 in the mucosal nerve fibres around a crypt (large arrows), in the submucosal nerve fibres (arrowheads) and ganglia (asterisks), and the neuronal somas (asterisks) and nerve fibres (small arrows) of the muscular layer of a 36-year-old patient with UC. (B) Representative photographs of P-α-syn staining in the mucosa (M), submucosa (SM) and muscularis externa (ME) from the colon of a control patient and a patient with UC. Neuronal structures are indicated as in (A). Scale bars: 20 μm (A) and 50 μm (B). (C) Quantification of fluorescence intensity (as arbitrary units) measured in the mucosa (M), submucosa (SM) and muscularis externa (ME); $N = 4–6$. Statistical analysis: Mann–Whitney *U*-test for independent samples, with $\alpha = 0.05$; *, $p < 0.05$ and **, $p < 0.01$ comparing the UC with the control group.

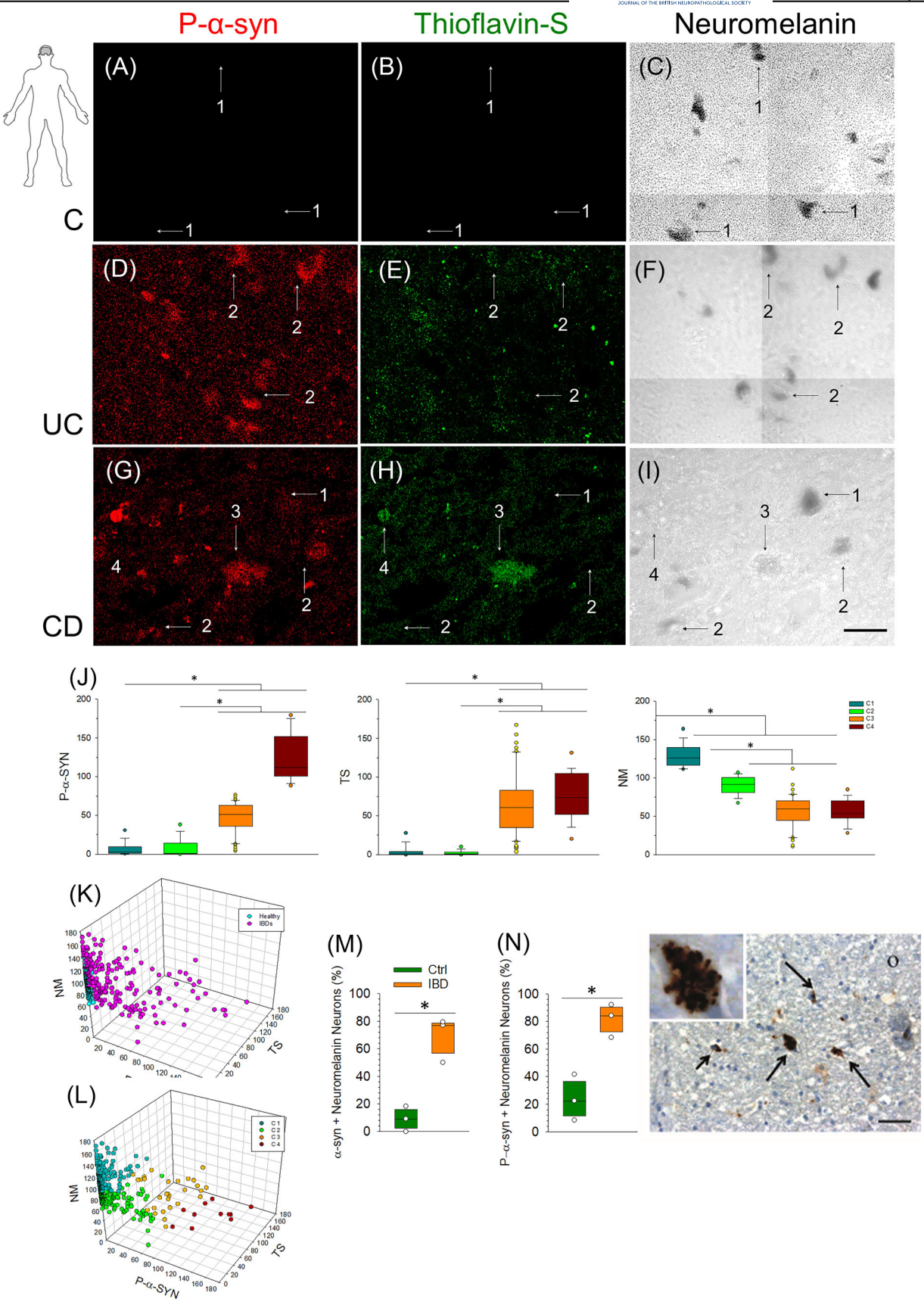


**FIGURE 2** Legend on next page.

The primer sequences for all the parameters studied are shown in Table S5. The cycle at which each sample crossed a fluorescence threshold, Ct, was determined, and the triplicate values for each cDNA were averaged. Analyses of RT-qPCR were performed using a comparative Ct method integrated into a Bio-Rad System Software. Additional details of this technique are available within the Supporting Information.

## Fourier-transform infrared (FTIR) spectroscopy

This technique allowed us to measure β-sheet structures and therefore help us to undertake a quantitative analysis of the α-syn aggregation. Background spectra were collected from a clean area of the same $CaF_2$ window. All measurements were made at RT. Brain sections, 15 μm thick, were cut on a cryostat (Leica CM 1850 UV) and mounted onto $CaF_2$ windows (Crystran). Analysis of FTIR spectra was performed using OPUS software (Bruker). The level of β-aggregation of proteins in the tissue was studied in the left and right SN by calculating the peak intensity ratio between 1620 and 1630 $cm^{-1}$, corresponding to β-sheet structures, and the maximum corresponding mainly to α-helical content at 1656 $cm^{-1}$. An increase in the 1620- to 1630-$cm^{-1}$ component was considered a signature of β-sheet structures [10]. Additional details of this technique are available within the Supporting Information.

## Histological score of colon

Paraffin-embedded sections of the colon were stained with haematoxylin/eosin. The analysis was performed in a blinded fashion by a validated method [11]. Colonic damage was graded on a scale of 0–3 based on destruction of epithelium, dilatation of crypts, loss of goblet cells, inflammatory cell infiltrate, oedema and crypt abscesses.

## Statistics

After analysing data normality by the Shapiro–Wilk test, groups were compared by one of the following tests when appropriated: the Kruskal–Wallis test for k-independent measures, followed by the Dunn's post hoc test; the Mann–Whitney *U*-test with a Bonferroni correction for post hoc pairwise comparisons; the Mann–Whitney test for two independent measures; the Friedman's test for *k*-related measures, with a Bonferroni correction for post hoc pairwise comparisons; or the Student–Newman–Keuls method. The hierarchical cluster analysis, followed by a *k*-means method, was used for the analysis of human mesencephalic neurons ($\alpha = 0.05$) using the IBM SPSS 26 software. All measurements were taken from distinct samples, except peripheral cell infiltration data, which were measured in a pool of tissue (Figure 5A–C). The whiskers and boxes representations show quartile 1 (25%), quartile 2 (50%, median) and quartile 3 (75%), as well as the 5th and 95th percentiles.

# RESULTS

## Detection of P-α-syn in the gut of human subjects with UC

We collected colon samples from six IBD subjects and six aged-matched controls (Table S1). P-α-syn accumulation in the inflamed colon of UC subjects was increased compared with controls (Figure 1). P-α-syn showed a significant increase in all layers of the colon wall (mucosa, submucosa and muscularis externa), compared with control subjects.

The colocalisation of P-α-syn with Ubiquitin C-terminal hydrolase L1 (UCHL-1) showed that P-α-syn was present in the ENS, in both myenteric and submucosal plexuses of IBD subjects. P-α-syn was in the mucosal nerve fibres around the crypts, in the submucosal neuronal somas and nerve fibres, and the neuronal somas and nerve fibres of the muscular layer.

## Pathological forms of α-syn aggregates in the ventral mesencephalon of human IBD brains

After establishing the existence of pathogenic α-syn in the inflamed gut of IBD patients, we evaluated whether a transition from physiological to pathological forms of α-syn (and therefore from healthy to altered neurons) was evident in the brains of IBD subjects. In the

**FIGURE 2** Analysis of mesencephalic neurons of healthy individuals and those affected by IBDs. (A–I) Photomicrographs from the SN of healthy control (A–C) and IBD subjects (D–I) showing neurons belonging to each of the four clusters. The left panels show immunofluorescence to P-α-syn (red), the central panels show fluorescence of thioflavin-S (green) and the right panels show bright fields with neuromelanin as dark structures. The numbers denote clusters 1 to 4. Scale bar: 50 μm. (J) Boxes and whiskers representation of the three parameters used. Statistical analysis: Kruskal–Wallis test for *k*-independent measures followed by the Mann–Whitney post hoc *U*-test for pairwise comparisons with a Bonferroni correction, with $\alpha = 0.05$. *, $p < 0.05$. (K) Three-dimensional representation of the neurons according to their values of P-α-syn, thioflavin-S (TS) and neuromelanin (NM) expressed as mean intensity. The neurons from healthy individuals are shown in cyan and those from individuals with IBDs in pink. (L) Three-dimensional representation of the neurons grouped in four clusters after a hierarchical cluster analysis following a k-means method. (M) Colocalisation analysis of neuromelanin-positive neurons labelled with α-syn. (N) Colocalisation analysis of neuromelanin-positive neurons labelled with P-α-syn. Results are mean ± SEM of $N = 3$ IBD or control subjects and are expressed as a percentage of dopaminergic neurons. Statistical analysis: Student–Newman–Keuls method, with $\alpha = 0.05$, *$p < 0.01$. (O) Representative immunohistochemical image (developed with DAB) from a patient of IBD, showing accumulation of α-syn (arrows). Scale bars: 40 μm. Abbreviations: C, control; UC, ulcerative colitis; CD, Crohn's disease.

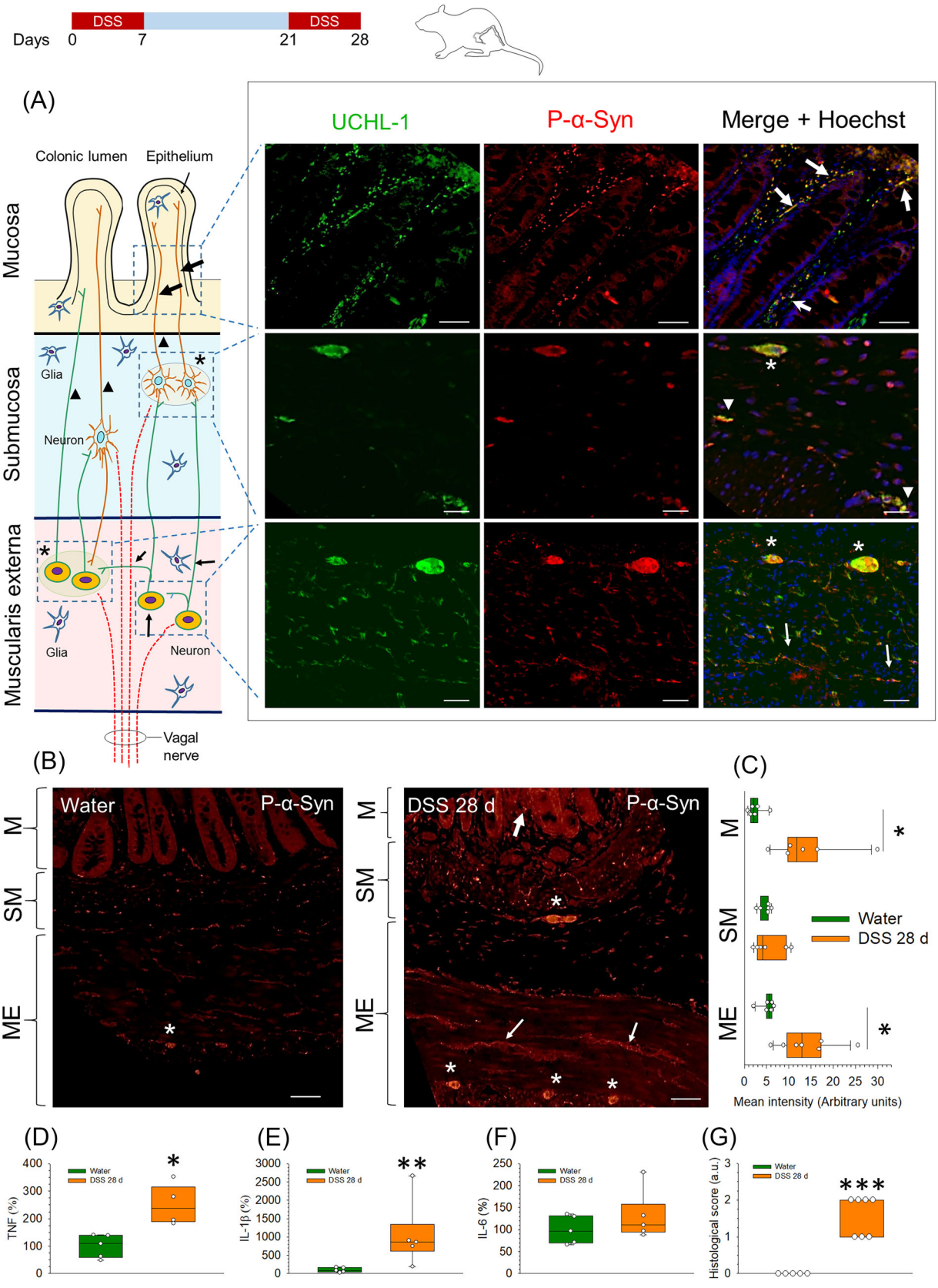


**FIGURE 3** Legend on next page.

human samples, dopaminergic neurons were first visualised by neuromelanin pigmentation. Early stages of α-syn pathology within nigral dopaminergic neurons include neuromelanin-related depigmentation and the appearance of 'pale bodies'. Remarkably, although neurons in the control subjects showed a normal pattern of neuromelanin pigmentation, we found clear displacement of neuromelanin in some neurons from the ventral mesencephalon in the eight IBD subjects, which was associated with the presence of α-syn aggregates reminiscent of pale bodies, which appear as critical elements preceding LB formation [12] (Figure 2 and Figures S2, S3, S4 and S5). The pathological nature of the aggregates was demonstrated by the presence of phosphorylated S129 α-syn, the form of α-syn most clearly associated with human synucleinopathies. Neurons from control subjects showed a normal pattern of α-syn, without inclusions. The expression of α-syn and P-α-syn in dopaminergic neurons showed an increase of 7.5- and 3.4-fold, respectively, compared with control human subjects (Figure 2).

Because pathogenic α-syn includes insoluble aggregates, we evaluated the levels of P-α-syn, thioflavin-S (insoluble aggregates) and neuromelanin in mesencephalic neurons from post mortem samples of healthy individuals and IBD patients (Figure 2 and Figures S3, S4 and S5). The hierarchical cluster analysis of these neurons suggested that they clustered in four different groups showing a gradient from healthy neurons characterised by low values of P-α-syn and thioflavin-S and high values of neuromelanin (clusters 1 and 2) to neurons characterised by high values of P-α-syn and thioflavin-S, and low values of neuromelanin (cluster 4), which could suggest altered functionality. Therefore, we found a clear association between P-α-syn, the formation of insoluble aggregates, and low levels of neuromelanin. Neurons from healthy individuals appear only in clusters 1 and 2, whereas neurons from IBD patients are found in all the clusters, indicating a wide range of neuronal functional states from healthy to damaged states in these patients. Finally, we evaluated the nature of the observed pathologies by immunostaining P-α-syn and ubiquitin on human brain sections (Figure S6). Notably, we found an increase in ubiquitin staining in IBD patients compared with controls. Furthermore, clear colocalisation was evident between P-α-syn and ubiquitin, two Lewy pathology markers.

## Phosphorylated α-syn in the gut of DSS-treated rats

We next wondered if inflamed gut in experimental animals triggers α-syn pathology in the GI system. We thus took advantage of a 28-day treatment with DSS in rats, an animal model of UC. Colon sections from these animals showed a significant increase in P-α-syn in the mucosa and muscular external layer of the colon compared with controls (Figure 3). The colocalisation of P-α-syn with the pan-neuronal marker UCHL-1 [13, 14] demonstrated that P-α-syn was present in the ENS, in both myenteric and submucosal plexuses of rats with DSS-induced colitis. P-α-syn was in the mucosal nerve fibres around the crypts and the neuronal somas and nerve fibres of either the submucosa or the muscular external layer.

RT-qPCR in DSS-treated rats showed an increase in TNF and IL-1β, whereas IL-6 showed no significant changes. Histological damage of the colon of DSS-treated animals showed a significant increase compared with control animals.

Serum levels of TNF and IL-1β significantly increased in animals completing DSS treatment (Figure S7a,b), corroborating that this treatment induced peripheral inflammation, an event associated, among others, with BBB permeability and brain infiltration of immune cells.

To extend our study, we also tested the effect of DSS treatment in a 63-day regimen. Gut analysis of α-syn pathology in the 63-day treatment showed alterations similar to those found in the 28-day treatment although the inflammatory markers in the colon were not different from control animals (Figure S8).

## BBB permeability and regional cerebral blood volume (rCBV) changes induced by DSS in rats

A single cohort of six rats underwent DSS treatment (7 days) and seven consecutive (daily) MRI sessions to assess BBB integrity. Day 0 represented the basal state of the BBB integrity and, thus, any MRI-based changes were compared with that time point thereafter (Figure 4). Significant increases in rCBV within the SN were observed at day 3 (2.8-fold compared with day 0), but no changes were found in the striatum. However, BBB disruption (as demonstrated by an increase in mean signal intensity on $T_1$-weighted images) was found in both the SN and striatum. BBB permeability increased in both regions and peaked at day 4.

## Peripheral immune cells infiltrate the brain of rats treated with DSS

Immune cell infiltration into brain parenchyma was analysed by FACS (Figure 5). 28-day DSS treatment increased the number of T

**FIGURE 3** Immunolocalisation of P-α-syn and upregulation of pro-inflammatory cytokines in the colon of rats under 28-day treatment with DSS. (A) Schematic cross-section of the colon wall illustrating the interconnected enteric plexuses, which contain neurons projecting to the mucosa, and vagal fibres. Colocalisation of UCHL-1 and P-α-syn in the mucosal nerve fibres around a crypt (large arrows), in the submucosal nerve fibres (arrowheads) and ganglia (asterisks), and the nerve fibres (small arrows) and ganglia (asterisks) of the muscular layer of a DSS-treated rat. (B) Representative photographs of P-α-syn staining in the mucosa (M), submucosa (SM) and muscularis externa (ME) from the colon of control (water) and DSS-treated rats. Neuronal structures are indicated as in (A). Scale bars: 20 μm (A) and 50 μm (B). (C) Quantification of P-α-syn staining fluorescence intensity (as arbitrary units) measured in the mucosa (M), submucosa (SM) and muscularis externa (ME); $N = 6–7$. (D, E, F) mRNA expression of TNF, IL1β and IL-6 quantified by RT-qPCR in the colon of control (water) and DSS-treated rats; $N = 4–5$. (G) Histological score of the colon of control (water) and DSS-treated rats; $N = 5–7$. Statistical analysis: Mann–Whitney *U*-test for independent samples, with $\alpha = 0.05$; *, $p < 0.05$, **, $p < 0.01$ and ***, $p < 0.001$, comparing the DSS-treated with the control (water) group.

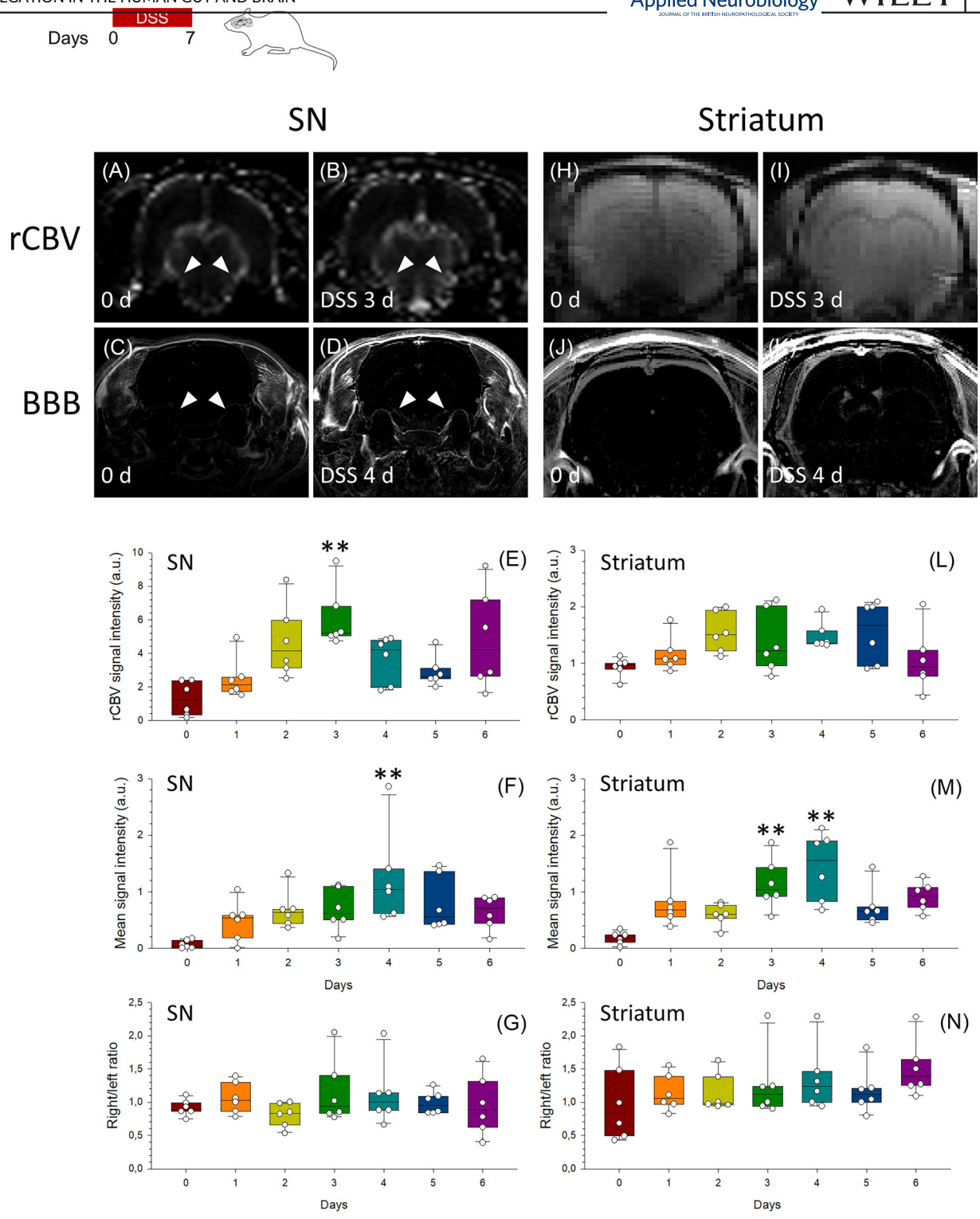


**FIGURE 4** MRI study of SN and striatum of rats under 28-day DSS treatment. Representative rCBV maps showing the signal coming from the blood vessels within the SN area after 0 (A) and 3 days (B) of DSS treatment. Comparison of post-gadolinium $T_1$-weighted images at day 0 (C) and day 4 (D) after DSS treatment show a clear enhancement within the SN 4 days after DSS treatment, suggesting changes in BBB structure and permeability. Arrowheads point SN. Quantification of rCBV within the SN (E) throughout the 6 days of DSS treatment. Quantification of the post–pre gadolinium-DTPA induced hyperintensity throughout DSS treatment within the SN (F). (G) Measurement of gadolinium-DTPA enhancement comparing right vs left SN of DSS-treated rats. Representative rCBV maps showing the signal coming from the blood vessels within the striatum area after 0 (H) and 3 days (I) of DSS treatment. Comparison of post-gadolinium $T_1$-weighted images at day 0 (J) and day 4 (K) after DSS treatment. Quantification of rCBV within the striatum (L) throughout the 6 days of DSS treatment. Quantification of the post-pre gadolinium-DTPA induced hyperintensity throughout DSS treatment within the striatum (M). (N) Measurement of gadolinium-DTPA enhancement comparing right vs left striatum of DSS-treated rats. $N = 6$. Statistical analysis: Friedman's test for $k$-related measures followed by a post hoc test for pairwise comparisons with a Bonferroni correction with $\alpha = 0.05$. **, $p < 0.01$, compared with day 0.

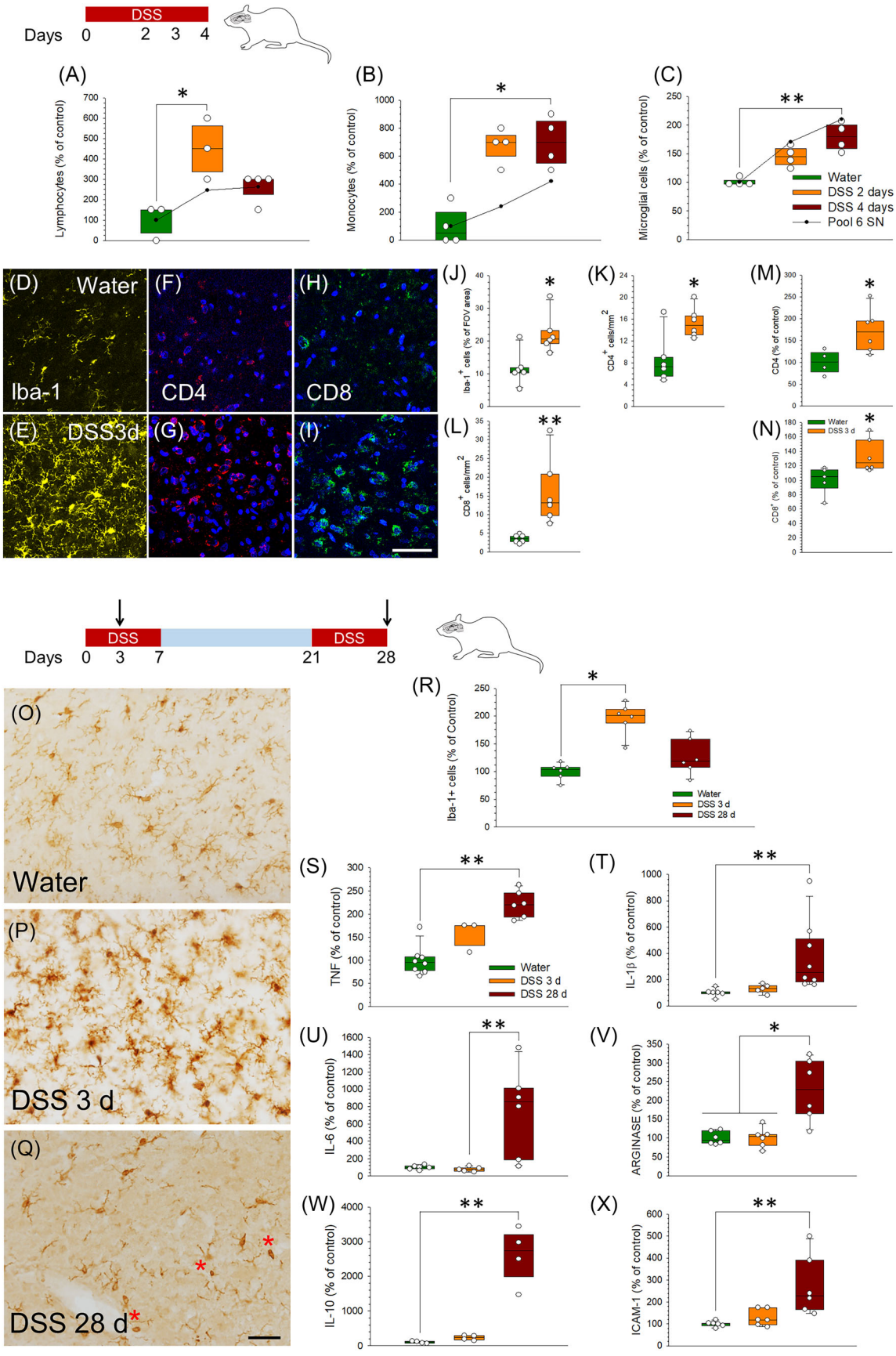


**FIGURE 5** Legend on next page.

lymphocytes at day 2, whereas the increase in monocyte infiltration was significantly altered at day 4. Microglial cell number was also increased at day 4 of DSS treatment. Further analysis by immunofluorescence and dot blot demonstrated a significant increase in microglial activation (Iba1), as well as numbers of $CD4^+$ and $CD8^+$ T lymphocytes within the SN 3 days after DSS treatment (Figure 5).

## Microglial activation in rats after treatment with DSS

The number of activated microglia/macrophages increased significantly at day 3 (Figure 5) and returned to control levels after 28-day DSS treatment; around 30% of cells retained the typical morphology of chronically activated microglia. Assessment of microglial morphology in the SN associated with different activation states in response to DSS treatment showed a progression from quiescent microglia to amoeboid-like activated cells (Figure S9).

We also studied the activation of microglial cells at the molecular level by RT-qPCR for TNF, IL-1β, IL-6, arginase and IL-10, as well as the expression of intercellular adhesion molecule (ICAM)-1 due to its role in cell infiltration. Interestingly, we found significant DSS-associated changes in the 28-day DSS treatment in all the mediators studied (Figure 5).

## Effects of DSS treatment on the ventral midbrain of rats

Quantification of TH-positive neurons in the SN of each animal after 28-day DSS treatment revealed a reduced number on the right side compared with the left side of DSS-treated animals and with control animals (Figure 6); this was confirmed in sections with TH-immunostaining and Nissl staining (Figure S10), indicating that treatment with DSS causes unilateral damage in the right SN. Dopaminergic arborisation (measured as the TH-stained area) following DSS treatment showed a decrease in the ventral mesencephalon (Figure 6). In addition, the intensity of α-syn staining in the TH-positive neurons was greater in the midbrain of DSS-treated rats as compared with controls, suggesting that α-syn aggregation in the brain could be affected under conditions of gut inflammation. We could detect some α-syn inclusions associated with swollen, light TH nigral degenerative fibres in response to DSS in both left and right SN, although more abundant on the right side. We also measured the abundance of β-sheet structures (presence of α-syn aggregates) in the SN of rats subjected to 28-day DSS treatment by FTIR spectroscopy, a typical feature of amyloid deposits. Contrary to control brains, levels of β-sheet structures were significantly elevated in the right SN from DSS-treated animals.

Further quantification of TH-positive neurons after a chronic 63-day treatment with DSS revealed that both the left and the right SN were affected (Figure S11). To confirm the presence of pathological α-syn in the ventral mesencephalon, we analysed the presence of P-α-syn by confocal microscopy. In control animals, α-syn staining was diffuse corresponding to a classical presynaptic localisation (Figure S12h–j). However, in DSS-treated animals, the presence of α-syn aggregates was mostly evident in dopaminergic processes (Figure S12k-m) but also in the soma (Figure S12g). This analysis demonstrated the existence of P-α-syn dopaminergic neuritic inclusions in response to chronic DSS treatment (Figures 11e and 12n–p). In addition, we analysed α-syn staining and dopaminergic arborisation using an immunofluorescence approach regardless of the hemisphere following chronic DSS treatment (Figure S11f). Overall, α-syn staining increased in the ventral mesencephalon of DSS-treated animals.

## Vagotomy effects on the DSS treatment

Vagotomy of control and 28-day DSS-treated animals (Figure 7) showed a clear protection of the dopaminergic system in vagotomised

**FIGURE 5** Effect of the DSS treatment on the infiltration of peripheral cells into the SN and the activation of microglia in the ventral mesencephalon of rats at both cellular and molecular levels. FACS analysis in the SN of control animals (water) and animals after 2 or 4 days of DSS treatment. Graphs show the percentage of lymphocytes (A), monocytes (B) and microglial cells (C) in the tissue sample. The results shown in the boxes and whiskers representations are expressed as a percentage of control from individual SN ($N = 3$ for the control and DSS 2 days groups of lymphocytes; $N = 4$ for the rest of the groups). The line and scatter plots represent a pool of $N = 6$ SN. Peripheral cell infiltration after 3 days of DSS treatment was confirmed by immunofluorescence of Iba-1 for microglial cells (D, E, J) and of $CD4^+$ (F, G, K) and $CD8^+$ (H, I, L) for lymphocytes. Scale bar: 50 μm. Results are expressed as percentage of microglial area per field of view (FOV), and number of $CD4^+$ and $CD8^+$ lymphocytes per $mm^2$, respectively. Panels M and N show dot blot analysis as a percentage of control. Coronal sections showing Iba-1 immunoreactivity in the SN. (O) Control animals. (P) Animals after 3 days of DSS. Note that DSS treatment increased microglial activation after 3 days. (Q) Animals after 28-day DSS treatment. Asterisks point to round phagocytic cells. Scale bars: O–Q, 50 μm. (R) Quantification of Iba-1-positive cells in the SN of rats. Results are expressed as a percentage of control; $N = 6$ for all groups. Effect of DSS on the expression of TNF (S), IL-1β (T), IL-6 (U), arginase (V), IL-10 (W) and ICAM-1 (X) mRNAs. mRNA expression in SN after 3 or 28 days of DSS intake was quantified by RT-qPCR. No significant changes were found after 3 days of treatment with DSS. Expression levels of TNF, IL-1β, IL-6, arginase, IL-10 and ICAM-1 increased after 28-day DSS treatment. Results are expressed as a percentage of control values; $N = 3$–8. Statistical analysis for panels A–C: Kruskal–Wallis test for *k*-independent measures followed by Dunn's post hoc test for pairwise comparisons with a Bonferroni correction, with $\alpha = 0.05$. Statistical analysis for panels J–N: Mann–Whitney *U*-test for independent samples, with $\alpha = 0.05$; *, $p < 0.05$ and **, $p < 0.01$ comparing the DSS with the control group. Statistical analysis for panels R–X: Kruskal–Wallis test for *k*-independent measures followed by Dunn's post hoc test for pairwise comparisons with Bonferroni's correction, with $\alpha = 0.05$. *, $p < 0.05$ and **, $p < 0.01$, compared with the control group. Abbreviations: DSS3d, 3 days of DSS; 28-day DSS, 28 days of DSS treatment.

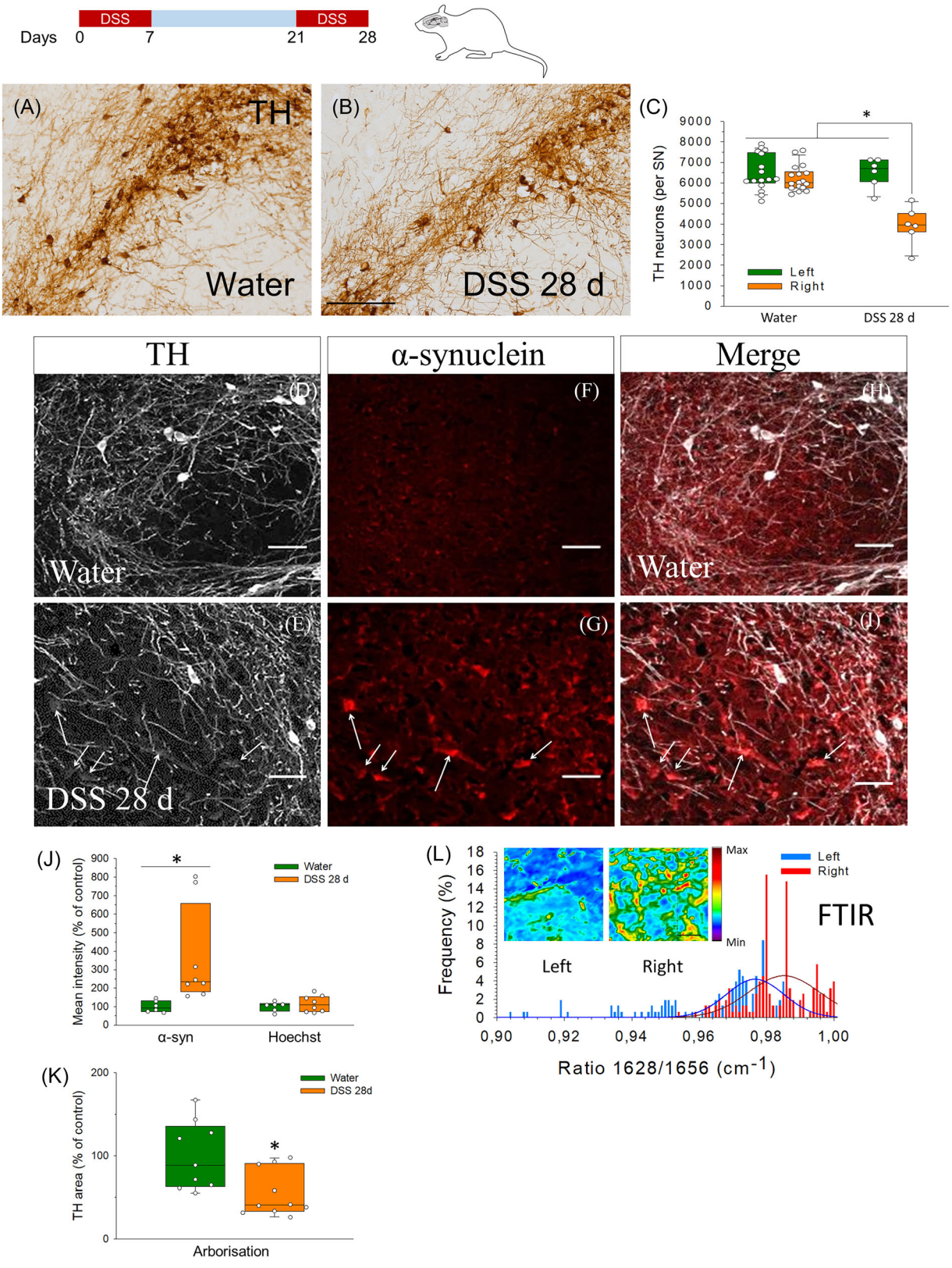


**FIGURE 6** Legend on next page.

rats compared with sham-operated animals in terms of number of TH-positive neurons and arborisation. We also found an increase in the intensity of α-syn in TH-positive neurons in the midbrain from DSS-treated sham-operated animals that was abolished in DSS-treated vagotomised animals. Quantitative analysis in the colon showed a significant increase of P-α-syn in the mucosa of sham-operated animals treated with DSS that was prevented by vagotomy. In the muscular layer, P-α-syn increased in the DSS-treated animals, both sham-operated and vagotomised, compared with the control animals. DSS treatment upregulated brain levels of inflammatory molecules such as TNF, IL-1β and IL-6 as well as the anti-inflammatory cytokine IL-10 compared with control animals, an effect prevented by vagotomy; arginase expression was not altered by DSS treatment. However, vagotomy did not prevent the upregulation of ICAM-1 by DSS.

## DISCUSSION

There is a vigorous debate within the PD community regarding the possible onset of pathology in the ENS in a subgroup of patients referred to as the 'body-first' subtype [15, 16]. Some argue that the disease does not originate in the ENS, as no cases of isolated gut Lewy pathology without CNS involvement have been documented [17, 18]. However, several studies employing intragastrointestinal injections of pathological α-syn fibrils have furnished compelling evidence in support of the body-first hypothesis [7, 19]. Given that GI inflammation appears to play a role in both initiating and progressing [20], we have analysed the GI tract of IBD human subjects to determine whether pathological α-syn is formed during the disease. Our analysis demonstrated the presence of pathogenic P-α-syn in Auerbach's and Meissner's plexuses in the human inflamed colon. Remarkably, these ENS locations matched those found in many PD subjects, even at early stages [21], supporting the importance of gut inflammation in promoting pathogenic α-syn aggregation in the GI tract, a potential route towards the brain. We also collected mesencephalic resections from different subjects affected by IBD and analysed levels of α-syn phosphorylation at Ser129, which is a robust marker of α-syn inclusion pathology. Thioflavin-S staining was also used to detect insoluble fibril formation [22]. Hierarchical cluster analysis identified four well-defined neuronal conditions in IBD subjects ranging from healthy melanized neurons lacking P-α-syn aggregation to highly depigmented neurons showing insoluble P-α-syn aggregates highly reminiscent of pale bodies. To the best of our knowledge, this is the first study demonstrating α-syn pathology within ventral midbrain dopaminergic neurons from patients earlier diagnosed with IBD and with an average age below 48 years. These stages of neuronal changes resemble the different steps leading to LB formation [23]. Typical features of the stages preceding LB appearance are poorly pigmented neurons containing α-syn cytoplasmic inclusions, similar to those reported here, including pale bodies [24, 25]. Depigmentation of nigral dopaminergic neurons is associated not only with early stages of α-syn but also with later stages of degeneration with obvious LB formation [26]. The same study also revealed that nigral dopaminergic neurons of normal morphological appearance and no characteristic pathology in PD exhibited significantly increased neuromelanin density [26]. These collective findings strongly suggest that the depigmentation of nigral dopaminergic neurons is a consistent feature observed throughout both the early and late stages of pathological α-syn aggregation. Overall, analysis of the human samples strongly supports the association between IBD and pathogenic α-syn aggregates in the ventral mesencephalon and reinforces the emerging association between gut disease and PD. The body-first hypothesis posits that α-syn pathology may propagate through the vagus nerve to reach the DMV and through sympathetic connections to the coeliac or mesenteric ganglia, subsequently extending to the sympathetic trunk and heart [15, 16, 19]. These investigations raise the intriguing possibility that not only the vagus nerve but also the sympathetic nervous system could potentially serve as a conduit for the dissemination of pathology to the CNS. Conducting systematic studies in these areas in the future will be imperative to assess whether there is an association between IBD and the presence of pathological α-syn in the sympathetic system.

To delve into the molecular mechanism that could underlie the spreading of pathogenic α-syn aggregation from the gut to the brain, we took advantage of a rodent experimental UC model based on the oral administration of DSS, a treatment that is known to induce a

**FIGURE 6** Effects of the treatment with DSS on the dopaminergic system and dendritic arborisation and expression of α-syn in the rat mesencephalon. TH immunohistochemistry illustrates a significant loss of dopaminergic neurons in the right SN from DSS-treated animals for 28 days (B) with respect to the control animals (A). Scale bars: 1 mm. (C) Quantification of TH-positive cells in the SN of rats. Results are expressed as the number of TH-positive neurons per SN. $N = 17$ for the water group and $N = 6$ for the DSS group. Statistical analysis: The Kruskal–Wallis test for $k$-independent measures followed by Dunn's post hoc test for pairwise comparisons with a Bonferroni correction with $\alpha = 0.05$: *, $p < 0.05$ compared with the other groups. (D, E) Representative microphotographs of immunofluorescence for TH (grey) in control (water) and DSS-treated rats. (F, G) Representative microphotographs of immunofluorescence for α-syn (red). The arrows indicate spots of accumulation of α-syn. (H, I) Merged images of TH and α-syn. The arrows indicate spots of accumulation of α-syn. Scale bars: 66 μm. (J) Quantification of α-syn and Hoechst intensity, and (K) arborisation using a section-by-section comparison between control and DSS-treated rats of the mean fluorescence intensity for these markers and TH area in SN for arborisation. Results are expressed as a percentage of control values for each parameter; $N = 6$–10. Statistical analysis: Mann–Whitney $U$-test for two independent samples, with $\alpha = 0.05$. *, $p < 0.05$ compared with the control group. (L) Histogram showing the levels of β-sheet structures (recorded as FTIR spectra) in the left and right SN of rats treated with DSS for 28 days. Results are expressed as the ratio β-sheet structures/total proteins (1628/1656 $cm^{-1}$); $N = 155$ for the left side and $N = 155$ for the right side (5 animals, 33 measures per animal for each side). Statistical analysis: Mann–Whitney $U$-test for independent measures, with $\alpha = 0.05$. $P$-value was 0.000 comparing the left with the right sides.

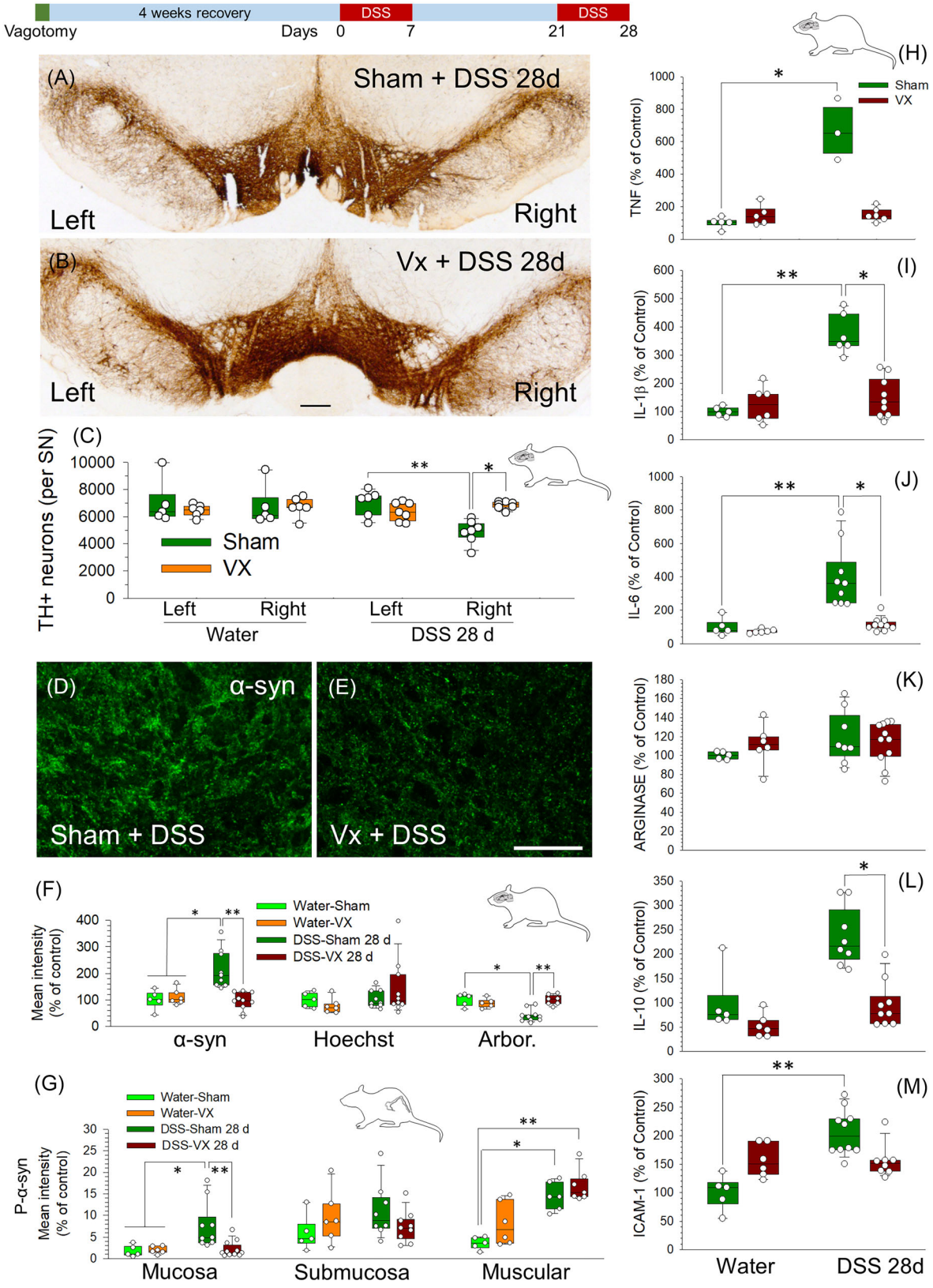


**FIGURE 7** Legend on next page.

strong gut inflammation. The gut analysis revealed pathogenic P-α-syn aggregates in the mucosal nerve fibres around the crypts, neuronal somas and nerve fibres of both the submucosa and the muscular external layer, a common pattern found in PD patients [27]. Subsequently, we analysed different features typically associated with peripheral inflammation. First, we performed MRI studies in rats under DSS treatment and analysed cerebrovascular functions and BBB integrity. Our results show that acute DSS induces a significant increase in rCBV together with a progressive increase in BBB permeability, in both the SN and striatum. Furthermore, changes in BBB permeability were accompanied by a significant upregulation of ICAM-1 mRNA levels in the SN, a cell adhesion molecule that participates in the attachment of leukocytes to the vascular endothelium and its subsequent extravasation [28]. Interestingly, this molecule has been suggested to sustain inflammation [29] and it is upregulated in PD [30]. Interestingly, a recent study has shown that BBB leakage increased in PD compared with control subjects with cerebrovascular disease and healthy control subjects. A significantly higher Ktrans was found in PD patients using dynamic contrast-enhanced MRI, and this was thought to reflect a higher BBB leakage than in the control group [31]. Our FACS, dot blot and confocal data suggested infiltration of peripheral monocytes and $CD4^+$ and $CD8^+$ lymphocytes at 2–4 days of DSS treatment when the BBB was altered. Interestingly, infiltrating cytotoxic $CD4^+$ and $CD8^+$ lymphocytes have been also observed in the inflamed SN of post mortem human PD [32, 33]. Analysis of microglia revealed an early morphological activation in the ventral mesencephalon in parallel with the BBB alteration, also mimicking PD features [34, 35].

We also analysed the integrity of the nigral dopaminergic system and α-syn expression in the ventral midbrain in the 28-day DSS rat model. Intriguingly, we found a loss of 40% of dopaminergic neurons in the right SN but no significant loss within the left SN. Asymmetry of dopaminergic neurodegeneration and subsequent lateralisation of motor symptoms are distinctive features of PD compared with other forms of neurodegenerative or symptomatic parkinsonism [36, 37]. However, the origin and role of this asymmetry in disease pathology are still not well understood and many research works and reviews have been published in recent years trying to provide a better understanding of this phenomenon with controversial results. Thus, although the α-Synuclein Origin site and Connectome (SOC) model proposes that PD cases, in which pathology begins in the peripheral autonomic nervous system (body-first subtype), would lead to more symmetric dopaminergic degeneration and less motor asymmetry [38], some experimental models found an intriguing asymmetry [39–42]. This asymmetry correlates with the innervation of the vagus nerve to the colon (right vagus nerve branch [43]) (Figure S13). In line with this anatomical distribution, some recent papers have found that the right branch of the vagus nerve affects preferentially the SN pars compacta [44, 45]. All these data support our findings and led us to subsequently analyse the secondary structure of proteins including β-sheet rich α-syn amyloid fibrils typically associated with LB and Lewy neurites [46] by FTIR in the DSS model. This analysis suggests the presence of β-sheet structures of α-syn that could eventually lead to the formation of aggregates and their preferential distribution in the right hemisphere of DSS-treated animals. Our results differ from other animal studies with injection of seeds into the gut/peritoneum that find symmetric alpha-synuclein pathology [47–49]. However, none of these papers use an inflammatory DSS model to induce alpha-syn misfolding/spreading. One possible explanation for the different results found in these papers could be due to the different time points assessed along with the above-mentioned asymmetry of the vagus nerve, which branches specifically innervate different parts of the gastrointestinal system, making it difficult to homogenise results that come from different experimental approaches.

To further validate our data, a new cohort of vagotomised animals underwent the DSS treatment. We found pathological P-α-syn in the gut, but neither TH-cell degeneration nor α-syn overexpression in the ventral mesencephalon. These results support the important role of the vagus nerve in spreading pathogenic forms of α-syn from the inflamed gut to the brain. Interestingly, vagotomy completely abrogated the long-term DSS-induced activation of key inflammatory markers in the ventral mesencephalon. However, an important non-mutually exclusive feature of IBD and DSS-based models of UC is peripheral inflammation. It is long known that systemic inflammation causes microglial activation, cytokine production and selective death of nigral dopaminergic neurons in different experimental models [50]. These events may have a significant contribution to dopaminergic pathology that needs to be further elucidated. Indeed, any condition accompanied by peripheral inflammation, including IBD, could present a risk factor for the significant neurodegeneration observed in PD [51].

Given the co-existence of gut and peripheral inflammation at the end of the DSS model and its relatively short duration (28 days), we decided to extend the duration of the DSS regime to a 63-day

**FIGURE 7** Effect of vagotomy on the changes induced in rats by the 28-day treatment with DSS. Coronal sections of TH immunohistochemistry showing the whole SN from (A) sham-operated and (B) vagotomised (Vx) animals, all of them treated with DSS. (C) Quantification of TH-positive cells in the SN of rats. Results are expressed as the number of TH-positive neurons per SN; $N = 5–7$. (D) Immunofluorescence shows an increase of α-syn in the SN of sham-operated animals treated with DSS that is reduced in the vagotomised rats (E). Scale bars: 1 mm (A and B) and 30 μm (D and E). (F) Quantification of the mean fluorescence intensity of α-syn, Hoechst and arborisation (Arbor.) as mean TH area in the SN of rats. Results are expressed as a percentage of control values for each parameter; $N = 5–10$. (G) Quantification of fluorescence intensity of P-α-syn (as arbitrary units) measured in the mucosa, submucosa and muscularis externa (muscular) in the colon of rats; $N = 5–11$. Effect of DSS and vagotomy on the expression of TNF (H), IL-1β (I), IL-6 (J), arginase (K), IL-10 (L) and ICAM-1 (M) mRNAs. mRNA expression was quantified by RT-qPCR. Although DSS treatment increased the levels of these molecules in sham-operated animals, this effect was abolished when animals were vagotomised; $N = 3–11$. Statistical analysis: Kruskal–Wallis test for *k*-independent measures followed by Dunn's post hoc test for pairwise comparisons with a Bonferroni correction, with $\alpha = 0.05$: *, $p < 0.05$ and **, $p < 0.01$.

treatment. With this second model, we wanted to study the long-term effects of α-syn pathology in the gut and brain under UC-related systemic inflammation. Gut analysis of α-syn pathology showed alterations similar to that found in the 28-day treatment. Further analysis of the ventral midbrain revealed a significant loss of TH dopaminergic neurons in both hemispheres. Therefore, we may conclude that in our experimental models (28- and 63-day DSS models), we found lesions of the nigral dopaminergic system that started unilaterally (28-day subchronic model) and then spread bilaterally (63-day chronic model), mimicking the natural progression of PD and a long-lasting α-syn pathology.

Our study adds to different pieces of evidence supporting the connection between IBD and PD (Figure S13) [9, 20, 52–54]. The demonstration of α-syn pathology in the gut and brain of IBD patients supports the bottom-up pathology hypothesis, thus the spreading of α-syn from submucosal neurons to the ventral midbrain, via the vagal preganglionic innervation of the gut. The results of the current study agree with epidemiological studies suggesting that truncal vagotomy is associated with a decreased risk of PD [55, 56]. The fact that only a small subset of IBD patients develop PD suggests that gut inflammation is a miscellaneous of risk factors including (i) bottom-up spreading of α-syn pathology, (ii) systemic inflammation causing BBB disruption, (iii) brain immune cell infiltration and (iv) microglia activation. Overall, our study revitalises the predicted importance of the GI tract in starting PD pathology and paves the way for different research strategies to define prodromal conditions and to identify novel early biomarkers of PD.

## AUTHOR CONTRIBUTIONS

Rocío M. de Pablos and José L. Venero designed the study and wrote the manuscript. Rocío M. de Pablos also carried out stereological analysis, and PCR experiments, analysed and interpreted the data. Ana M. Espinosa-Oliva performed the animal treatments, perfusions and dissection of animal brains. She also carried out immunohistochemistry and ELISA assays and was also involved in drafting and revising the manuscript. Manuel Sarmiento Soto, Sébastien Serres and Vasiliki Economopoulus performed MRI studies. Manuel Sarmiento Soto and Rocío Ruiz performed and analysed immunofluorescence assays from rat and human brains. Antonio Boza-Serrano contributed to the immunohistochemistry assays, PCR and sample preparation for FTIR. Ana I. Rodriguez-Perez performed bilateral sub-diaphragmatic vagotomies. María A. Roca-Ceballos helped with the immunofluorescence and immunohistochemistry techniques. Juan García-Revilla helped with the PCR experiments. Marti Santiago performed the HPLC assay. Ana E. Carvajal, María D. Vázquez-Carretero, Pablo García-Miranda and María J. Pera performed immunohistological assays from human and rat colon. María J. Pera also contributed to the analysis and interpretation of results. Oxana Klementieva carried out the FTIR study. María J. Oliva-Martín and Manuel Sarmiento Soto performed the flow cytometry assay. Eloy Rivas did the neuropathology analysis of the human brains. Alberto Machado contributed to the design and conceiving of the manuscript. Antonio J. Herrera contributed to statistical study, analysis and representation of data and writing of the manuscript. José L. Labandeira-García, Tomas Deierborg and Nicola R. Sibson were involved in critical revision of the manuscript. All authors participated in the discussion of the results and provided comments or edits to the manuscript. All authors read and approved the final manuscript.

## ACKNOWLEDGEMENTS

This work was supported by grants from the Spanish Ministerio de Economía y Competitividad (SAF2015-64171-R) and the Spanish Ministerio de Ciencia, Innovación y Universidades (RTI2018-098830-B-I00). AIRP and JLLG were funded by a grant of the Spanish Ministerio de Salud (PI17/00828). MSS, SS and NRS were funded by Cancer Research UK (grant number C5255/A15935). VE was funded by a Marie Skłodowska-Curie Individual Fellowship. MJP, MDVC and PGM were supported by a grant from the Junta de Andalucía (CTS 5884) and thank Prof. Dr. A.A. Ilundáin for the support provided. The authors thank the donors and the Biobanks (Principado de Asturias BioBank (PT17/0015/0023), the University Hospital Virgen del Rocío (HUVR)-IBiS Biobank (Andalusian Public Health System Biobank and ISCIII-Red de Biobancos: ISCCII-PT13/0010/0056), HUVR-IBiS Biobank (PT17/0015/0041), Biobank Hospital Universitario Puerta del Hierro Majadahonda (HUPHM/Instituto de Investigación Sanitaria Puerta del Hierro-Segovia de Arana (IDIPHISA)(PT17/0015/0020), HCB-IDIBAPS Biobank and the Oxford Brain Bank (OBB; OBB 453) for providing the human samples and for the assessment and technical support provided. Images were obtained in the Centro de Investigación, Tecnología e Innovación de la Universidad de Sevilla (CITIUS).

## CONFLICT OF INTEREST STATEMENT

The authors report no competing interest.

## PEER REVIEW

The peer review history for this article is available at https://www.webofscience.com/api/gateway/wos/peer-review/10.1111/nan.12962.

## DATA AVAILABILITY STATEMENT

The data that support the findings of this study are available from the corresponding author upon reasonable request.

## ETHICS STATEMENT

Human studies were approved by the corresponding ethic committees (authorisation code: 2051-N-20). Informed consent was obtained from all subjects.

## ORCID

*José L. Labandeira-García* https://orcid.org/0000-0002-8243-9791

## REFERENCES

1. Obeso JA, Rodríguez-Oroz MC, Rodríguez M, et al. Pathophysiology of the basal ganglia in Parkinson's disease. *Trends Neurosci*. 2000; 23(10 Suppl):S8-S19. doi:10.1016/S1471-1931(00)00028-8
2. Spillantini MG, Schmidt ML, Lee VM, et al. Alpha-synuclein in Lewy bodies. *Nature*. 1997;388(6645):839-840. doi:10.1038/42166

3. Braak H, Sastre M, Bohl JR, et al. Parkinson's disease: lesions in dorsal horn layer I, involvement of parasympathetic and sympathetic pre- and postganglionic neurons. *Acta Neuropathol*. 2007;113(4):421-429. doi:10.1007/s00401-007-0193-x
4. Holmqvist S, Chutna O, Bousset L, et al. Direct evidence of Parkinson pathology spread from the gastrointestinal tract to the brain in rats. *Acta Neuropathol*. 2014;128(6):805-820. doi:10.1007/s00401-014-1343-6
5. Manfredsson FP, Luk KC, Benskey MJ, et al. Induction of alpha-synuclein pathology in the enteric nervous system of the rat and non-human primate results in gastrointestinal dysmotility and transient CNS pathology. *Neurobiol Dis*. 2018;112:106-118. doi:10.1016/j.nbd.2018.01.008
6. Uemura N, Yagi H, Uemura MT, Hatanaka Y, Yamakado H, Takahashi R. Inoculation of alpha-synuclein preformed fibrils into the mouse gastrointestinal tract induces Lewy body-like aggregates in the brainstem via the vagus nerve. *Mol Neurodegener*. 2018;13(1):21. doi:10.1186/s13024-018-0257-5
7. Kim S, Kwon S-H, Kam T-I, et al. Transneuronal propagation of pathologic alpha-synuclein from the gut to the brain models Parkinson's disease. *Neuron*. 2019;103(627–641):e627.
8. Zhu F, Li C, Gong J, Zhu W, Gu L, Li N. The risk of Parkinson's disease in inflammatory bowel disease: a systematic review and meta-analysis. *Dig Liver Dis*. 2019;51(1):38-42. doi:10.1016/j.dld.2018.09.017
9. Kim GH, Lee YC, Kim TJ, et al. Risk of neurodegenerative diseases in patients with inflammatory bowel disease: a nationwide population-based cohort study. *J Crohns Colitis*. 2022;16(3):436-443. doi:10.1093/ecco-jcc/jjab162
10. Ami D, Lavatelli F, Rognoni P, et al. In situ characterization of protein aggregates in human tissues affected by light chain amyloidosis: a FTIR microspectroscopy study. *Sci Rep*. 2016;6(1):29096. doi:10.1038/srep29096
11. Cooper HS, Murthy SN, Shah RS, Sedergran DJ. Clinicopathologic study of dextran sulfate sodium experimental murine colitis. *Lab Invest*. 1993;69(2):238-249.
12. Fares MB, Jagannath S, Lashuel HA. Reverse engineering Lewy bodies: how far have we come and how far can we go? *Nat Rev Neurosci*. 2021;22(2):111-131. doi:10.1038/s41583-020-00416-6
13. Wilkinson KD, Lee KM, Deshpande S, Duerksen-Hughes P, Boss JM, Pohl J. The neuron-specific protein PGP 9.5 is a ubiquitin carboxyl-terminal hydrolase. *Science*. 1989;246(4930):670-673. doi:10.1126/science.2530630
14. Day IN, Thompson RJ. UCHL1 (PGP 9.5): neuronal biomarker and ubiquitin system protein. *Prog Neurobiol*. 2010;90(3):327-362. doi:10.1016/j.pneurobio.2009.10.020
15. Borghammer P, Horsager J, Andersen K, et al. Neuropathological evidence of body-first vs. brain-first Lewy body disease. *Neurobiol Dis*. 2021;161:105557. doi:10.1016/j.nbd.2021.105557
16. Borghammer P. The brain-first vs. body-first model of Parkinson's disease with comparison to alternative models. *J Neural Transm (Vienna)*. 2023;130(6):737-753. doi:10.1007/s00702-023-02633-6
17. Adler CH, Beach TG. Neuropathological basis of nonmotor manifestations of Parkinson's disease. *Mov Disord*. 2016;31(8):1114-1119. doi:10.1002/mds.26605
18. Beach TG, Adler CH, Sue LI, et al. Vagus nerve and stomach synucleinopathy in Parkinson's disease, incidental Lewy body disease, and normal elderly subjects: evidence against the "body-first" hypothesis. *J Parkinsons Dis*. 2021;11(4):1833-1843. doi:10.3233/JPD-212733
19. Van Den Berge N, Ferreira N, Gram H, et al. Evidence for bidirectional and trans-synaptic parasympathetic and sympathetic propagation of alpha-synuclein in rats. *Acta Neuropathol*. 2019;138(4):535-550. doi:10.1007/s00401-019-02040-w
20. Rolli-Derkinderen M, Leclair-Visonneau L, Bourreille A, Coron E, Neunlist M, Derkinderen P. Is Parkinson's disease a chronic low-grade inflammatory bowel disease? *J Neurol*. 2020;267(8):2207-2213. doi:10.1007/s00415-019-09321-0
21. Wakabayashi K, Takahashi H, Ohama E, Ikuta F. Parkinson's disease: an immunohistochemical study of Lewy body-containing neurons in the enteric nervous system. *Acta Neuropathol*. 1990;79(6):581-583. doi:10.1007/BF00294234
22. Maries E, Dass B, Collier TJ, Kordower JH, Steece-Collier K. The role of alpha-synuclein in Parkinson's disease: insights from animal models. *Nat Rev Neurosci*. 2003;4(9):727-738. doi:10.1038/nrn1199
23. Dale GE, Probst A, Luthert P, Martin J, Anderton BH, Leigh PN. Relationships between Lewy bodies and pale bodies in Parkinson's disease. *Acta Neuropathol*. 1992;83(5):525-529. doi:10.1007/BF00310030
24. Kastner A, Hirsch EC, Lejeune O, Javoy-Agid F, Rascol O, Agid Y. Is the vulnerability of neurons in the substantia nigra of patients with Parkinson's disease related to their neuromelanin content? *J Neurochem*. 1992;59(3):1080-1089. doi:10.1111/j.1471-4159.1992.tb08350.x
25. Wakabayashi K, Tanji K, Odagiri S, Miki Y, Mori F, Takahashi H. The Lewy body in Parkinson's disease and related neurodegenerative disorders. *Mol Neurobiol*. 2013;47(2):495-508. doi:10.1007/s12035-012-8280-y
26. Halliday GM, Ophof A, Broe M, et al. Alpha-synuclein redistributes to neuromelanin lipid in the substantia nigra early in Parkinson's disease. *Brain*. 2005;128(11):2654-2664. doi:10.1093/brain/awh584
27. Bindas AJ, Kulkarni S, Koppes RA, Koppes AN. Parkinson's disease and the gut: models of an emerging relationship. *Acta Biomater*. 2021;132:325-344. doi:10.1016/j.actbio.2021.03.071
28. Springer TA. Traffic signals for lymphocyte recirculation and leukocyte emigration: the multistep paradigm. *Cell*. 1994;76(2):301-314. doi:10.1016/0092-8674(94)90337-9
29. McGeer EG, McGeer PL. The role of anti-inflammatory agents in Parkinson's disease. *CNS Drugs*. 2007;21(10):789-797. doi:10.2165/00023210-200721100-00001
30. Sawada M, Imamura K, Nagatsu T. Role of cytokines in inflammatory process in Parkinson's disease. *J Neural Transm Suppl*. 2006;(70):373-381.
31. Al-Bachari S, Naish JH, Parker GJM, et al. Blood-brain barrier leakage is increased in Parkinson's disease. *Front Physiol*. 2020;11:593026. doi:10.3389/fphys.2020.593026
32. Brochard V, Combadiére B, Prigent A, et al. Infiltration of CD4+ lymphocytes into the brain contributes to neurodegeneration in a mouse model of Parkinson disease. *J Clin Invest*. 2009;119(1):182-192. doi:10.1172/JCI36470
33. Ferrari CC, Tarelli R. Parkinson's disease and systemic inflammation. *Parkinsons Dis*. 2011;2011:436813.
34. McGeer PL, McGeer EG. Inflammation and neurodegeneration in Parkinson's disease. *Parkinsonism Relat Disord*. 2004;10(Suppl 1):S3-S7. doi:10.1016/j.parkreldis.2004.01.005
35. Tiwari PC, Pal R. The potential role of neuroinflammation and transcription factors in Parkinson disease. *Dialogues Clin Neurosci*. 2017;19(1):71-80. doi:10.31887/DCNS.2017.19.1/rpal
36. Thenganatt MA, Louis ED. Distinguishing essential tremor from Parkinson's disease: bedside tests and laboratory evaluations. *Expert Rev Neurother*. 2012;12(6):687-696. doi:10.1586/ern.12.49
37. Riederer P, Sian-Hulsmann J. The significance of neuronal lateralisation in Parkinson's disease. *J Neural Transm (Vienna)*. 2012;119(8):953-962. doi:10.1007/s00702-012-0775-1
38. Borghammer P. The α-synuclein origin and connectome model (SOC model) of Parkinson's disease: explaining motor asymmetry, non-motor phenotypes, and cognitive decline. *J Parkinsons Dis*. 2021;11(2):455-474. doi:10.3233/JPD-202481
39. Miwa H, Kubo T, Suzuki A, Kondo T. Intragastric proteasome inhibition induces alpha-synuclein-immunopositive aggregations in neurons in the dorsal motor nucleus of the vagus in rats. *Neurosci Lett*. 2006;401(1-2):146-149. doi:10.1016/j.neulet.2006.03.003

40. Van Kampen JM, Baranowski DC, Robertson HA, et al. The progressive BSSG rat model of Parkinson's: recapitulating multiple key features of the human disease. *PLoS ONE*. 2015;10(10): e0139694. doi:10.1371/journal.pone.0139694
41. Taherianfard M, Riyahi M, Razavi M, Bavandi Z, Eskandari Roozbahani N, Namavari MM. The cataleptic, asymmetric, analgesic, and brain biochemical effects of Parkinson's disease can be affected by toxoplasma gondii infection. *Biomed Res Int*. 2020;2020:2546365. doi:10.1155/2020/2546365
42. Morley V, Dolt KS, Alcaide-Corral CJ, et al. In vivo18F-DOPA PET imaging identifies a dopaminergic deficit in a rat model with a G51D α-synuclein mutation. *Front Neurosci*. 2023;17:1095761. doi:10.3389/fnins.2023.1095761
43. Drake RL, Mitchell AWM, Richard T, et al. *Gray's Atlas of Anatomy*. Vol. pp Xvi. Churchill Livingstone; 2008.
44. Han W, Tellez LA, Perkins MH, et al. A neural circuit for gut-induced reward. *Cell*. 2018;175(3):887-888. doi:10.1016/j.cell.2018.10.018
45. Cao Y, Li R, Bai L. Vagal sensory pathway for the gut-brain communication. *Semin Cell Dev Biol*. 2023;7:S1084-9521(23):00145-00143.
46. Araki K, Yagi N, Ikemoto Y, et al. Synchrotron FTIR micro-spectroscopy for structural analysis of Lewy bodies in the brain of Parkinson's disease patients. *Sci Rep*. 2015;5(1):17625. doi:10.1038/srep17625
47. Breid S, Bernis ME, Babila JT, Garza MC, Wille H, Tamgüney G. Neuroinvasion of α-synuclein prionoids after intraperitoneal and intraglossal inoculation. *J Virol*. 2016;90(20):9182-9193. doi:10.1128/JVI.01399-16
48. Lohmann S, Bernis ME, Tachu BJ, Ziemski A, Grigoletto J, Tamgüney G. Oral and intravenous transmission of α-synuclein fibrils to mice. *Acta Neuropathol*. 2019;138(4):515-533. doi:10.1007/s00401-019-02037-5
49. Van Den Berge N, Ferreira N, Mikkelsen TW, et al. Ageing promotes pathological alpha-synuclein propagation and autonomic dysfunction in wild-type rats. *Brain*. 2021;144(6):1853-1868. doi:10.1093/brain/awab061
50. Qin L, Wu X, Block ML, et al. Systemic LPS causes chronic neuroinflammation and progressive neurodegeneration. *Glia*. 2007;55(5): 453-462. doi:10.1002/glia.20467
51. Herrera AJ, Espinosa-Oliva AM, Oliva-Martin MJ, Carrillo-Jimenez A, Venero J, de Pablos R. Collateral damage: contribution of peripheral inflammation to neurodegenerative diseases. *Curr Top Med Chem*. 2015; 15(21):2193-2210. doi:10.2174/1568026615666150610142027
52. Lin JC, Lin CS, Hsu C, et al. Association between Parkinson's disease and inflammatory bowel disease: a nationwide Taiwanese retrospective cohort study. *Inflamm Bowel Dis*. 2016;22(5):1049-1055. doi:10.1097/MIB.0000000000000735
53. Peter I, Dubinsky M, Bressman S, et al. Anti-tumor necrosis factor therapy and incidence of Parkinson disease among patients with inflammatory bowel disease. *JAMA Neurol*. 2028;75(8):939-946. doi:10.1001/jamaneurol.2018.0605
54. Weimers P, Halfvarson J, Sachs MC, et al. Inflammatory bowel disease and Parkinson's disease: a nationwide Swedish cohort study. *Inflamm Bowel Dis*. 2019;25(1):111-123. doi:10.1093/ibd/izy190
55. Liu B, Fang F, Pedersen NL, et al. Vagotomy and Parkinson disease: a Swedish register-based matched-cohort study. *Neurology*. 2017; 88(21):1996-2002. doi:10.1212/WNL.0000000000003961
56. Svensson E, Horváth-Puhó E, Thomsen RW, et al. Vagotomy and subsequent risk of Parkinson's disease. *Ann Neurol*. 2015;78(4): 522-529. doi:10.1002/ana.24448


## SUPPORTING INFORMATION

Additional supporting information can be found online in the Supporting Information section at the end of this article.

**How to cite this article:** Espinosa-Oliva AM, Ruiz R, Soto MS, et al. Inflammatory bowel disease induces pathological α-synuclein aggregation in the human gut and brain. *Neuropathol Appl Neurobiol*. 2024;50(1):e12962. doi:10.1111/nan.12962